CHEMISTRY
A EUROPEAN JOURNAL

FULL PAPER

DOI: 10.1002/chem.201203247

Nanoscale Assembly of Paramagnetic Organic Radicals on Au(111) Single Crystals

Sabine-Antonia Savu,[a] Indro Biswas,[a] Lorenzo Sorace,[b] Matteo Mannini,[b] Donella Rovai,[b] Andrea Caneschi,[b] Thomas Chassé,[a] and Maria Benedetta Casu*[a]

Abstract: The successful thin-film deposition of a pyrene-substituted nitronyl nitroxide radical under controlled conditions has been demonstrated. The electronic properties, chemical environment at the interface, and morphology of the thin films have been investigated by a multitechnique approach. Spectroscopic and morphological analyses indicate a Stranski–Krastanov growth mode and weak physisorption of molecules onto the metallic surface. Electron spin resonance (ESR) spectroscopy shows that evaporation processes and deposition do not affect the paramagnetic character of the molecules. Useful concepts for the engineering of new, purely organic-based magnets, which may open the way to fruitful exploitation of organic molecular-beam deposition for assembly on solid surfaces in view of future technological applications, are presented.

Keywords: electron spin resonance · EPR spectroscopy · magnetism · nitronyl nitroxides · organic radicals · thin films · X-ray absorption spectroscopy

Introduction

Nucleation and growth processes in thin films have been the focus of intense investigation since the early 1950s because controlling nanoscale growth is essential to the development of applied materials in fields ranging from medicine to electronics.[1–7] Growth in the nanoscale regime has been extensively studied since the 1990s for atomistic growth of inorganic materials.[4–7] On the other hand, during the last two decades, molecular systems have proven to be excellent candidates for applications in innovative devices,[8] justifying extensive research activity in materials science, chemistry, and physics. To develop a strategic use of a new functional molecule in a nanoscale assembly, it is crucial to rationalize and tune its properties by influencing its growth modes. Indeed, it is known that intermolecular interactions, molecule–surface interactions, and substrate temperature play a role in determining the properties of films,[9,10] whereas preparation parameters influence nucleation and island dimensions.[11,12] Finally, substrate atomic topography and morphology strongly influence molecular arrangement within the film.[13,14] This structural property can also be tuned by varying the preparation parameters.[9–12]

This knowledge can be usefully applied to the nanostructuration of molecular magnets.[15–20] With the aim of establishing suitable strategies for layer growth and characterization of molecular magnetic systems, we focused our interest on the thin-film deposition of nitronyl nitroxide radicals. This class of paramagnetic compounds,[21–27] bearing unpaired electrons localized mainly in the two NO groups, has been widely studied in molecular magnetism, not only because of their intrinsic magnetic properties,[21] but also because of their use as a building block in more complex magnetic structures[26] and their rich redox chemistry, which may be applicable to memory elements.[28]

In the past, only rare attempts to study the evaporation of this class of molecules have been reported.[29–31] These efforts were focused on the archetypal *para*-nitrophenyl nitronyl nitroxide because of its purely organic ferromagnetism at ultra-low temperatures,[21] and dealt with thick films (in the micrometer range) characterized by crystal packings that emulate those of the different bulk phases. Our idea takes this approach further by focusing on deposition of (sub)nanometer-sized assemblies in a controlled environment to move toward potential use of such spin-carriers in spintronics, memory devices, and sensing materials.[18,19,27] These applications cannot be implemented without precise knowledge of the surface and thin-film processes and of the interface between the organic radicals and possible materials of technological interest like gold, oxides, and graphene.[18]

Herein, we report the successful growth of thin films of a pyrene derivative of the nitronyl nitroxide radical (4,4,5,5-tetramethyl-2-(pyrenyl)imidazoline-1-oxy-3-oxide, **NitPyn**,

[a] S.-A. Savu, Dr. I. Biswas, Prof. T. Chassé, Dr. M. B. Casu
Institute of Physical and Theoretical Chemistry
University of Tuebingen, Auf der Morgenstelle 18
72076 Tuebingen (Germany)
Fax: (+49) 7071-29-5490
E-mail: benedetta.casu@uni-tuebingen.de

[b] Dr. L. Sorace, Dr. M. Mannini, D. Rovai, Prof. A. Caneschi
Department of Chemistry "U. Schiff" and INSTM RU
University of Florence, Via della Lastruccia 3
50019 Sesto Fiorentino, FI (Italy)

Supporting information for this article is available on the WWW under http://dx.doi.org/10.1002/chem.201203247.

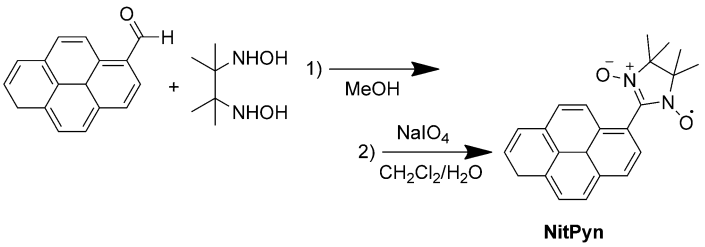

Scheme 1. Synthesis and molecular structure of **NitPyn**.

Scheme 1) by organic molecular-beam deposition (OMBD) under ultra-high vacuum conditions (UHV) on Au(111) single crystals. This specific derivative has been chosen because its pendent polyaromatic moiety may be suitable for assembly on metallic surfaces (e.g., gold) and carbon-based surfaces of technological relevance (e.g., carbon nanotubes and graphene).

NitPyn has been synthesized by following the general procedure for preparation of nitronyl nitroxide radicals[22] based on the condensation of the corresponding polyaromatic aldehyde with the appropriate dihydroxydiamine, followed by oxidation with periodate and a workup by column chromatography (see Scheme 1 and the Experimental Section).

The UHV compatibility of this novel radical derivative has been validated and detailed investigations into its thin-film growth on Au(111) down to the monolayer regime and its interface with gold have been carried out. The thin-film electronic structure and the interaction with the substrate have been investigated by X-ray photoelectron spectroscopy (XPS) and atomic force microscopy (AFM). Electron spin resonance (ESR) measurements have been performed to investigate the effects of evaporation and deposition on the magnetic characteristics of the molecule.

Results and Discussion

In Figure 1, the thickness-dependent C 1s, N 1s, and O 1s core-level photoemission spectra of **NitPyn** deposited on Au(111) single crystals at room temperature are shown. Precise information on film stoichiometry can be obtained from the analysis of the XPS spectra.[33,34] The ratio of the integrated signal intensities of the different lines of the XPS curves agree perfectly with the theoretical percentages expected on the basis of **NitPyn** stoichiometry, indicating that the deposition occurs without degradation (see Table S1 in the Supporting Information).

This result was confirmed by acquiring the same spectra of a **NitPyn** powder embedded in indium foil without evaporation (Figure 2). A comparison of the XPS signals of these two systems does not reveal any relevant energy shift or changes in lineshape (a slight broadening of the XPS lines and the small binding-energy differences of approximately 0.1 eV with respect to the thin film for the C 1s and N 1s core-level spectra, and 0.3 eV for the O 1s core-level spectra

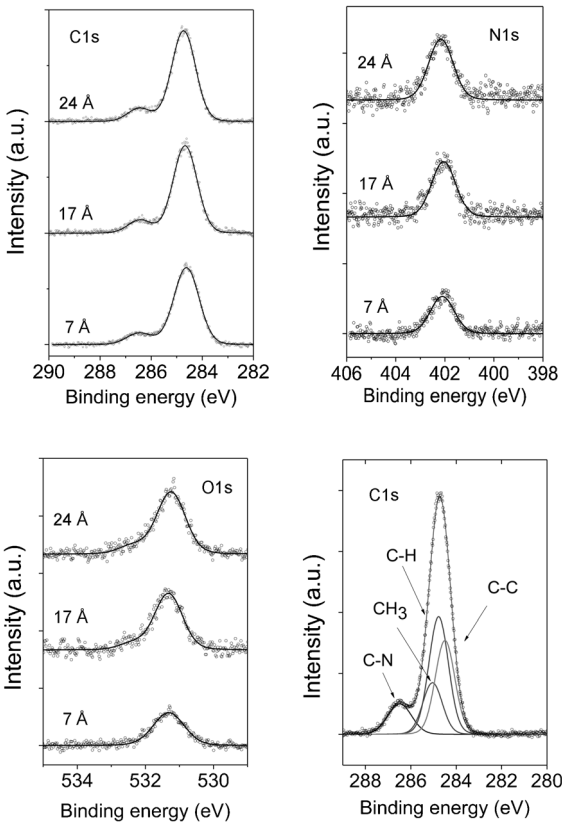

Figure 1. Thickness-dependent C 1s, N 1s (top left and right, respectively) and O 1s (bottom left) core-level photoemission spectra of **NitPyn** thin films deposited on Au(111) at room temperature. Bottom right: Peak-fitting analysis performed on the C 1s signal for a thicker film (24 Å).

are observed in the spectra of the powder because of typical charging phenomena occurring in photoemission in organic crystals). The additional signals detected in the C 1s and O 1s regions were assigned to indium carbide and indium

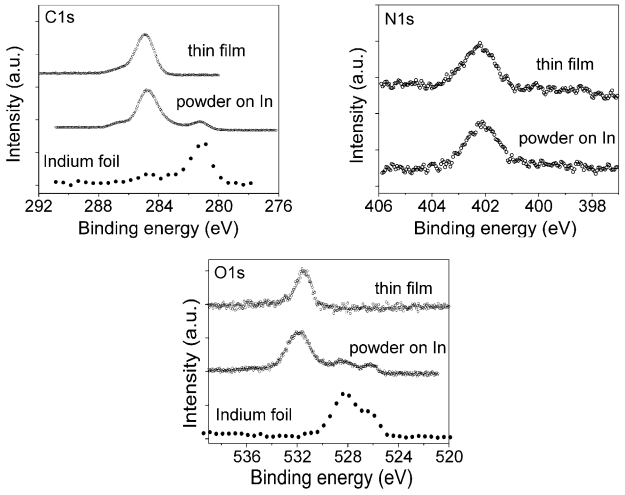

Figure 2. Comparison of the C 1s (top left), N 1s (top right), and O 1s (bottom) core-level XPS of a **NitPyn** thin film (49 Å nominal thickness), **NitPyn** powder deposited on indium foil, and indium foil stored under ambient conditions.

oxide present as contaminants in the supporting indium foil due to storage under ambient conditions prior to preparation.

The XPS fine structures are quantitatively interpreted on the basis of a peak-fit analysis, which allows the assignment of the principal photoemission lines, thus providing the binding energies of the core levels of chemically different atoms and corresponding information regarding bonding and screening processes.[32,33] Each chemically inequivalent carbon site should, in principle, yield a different contribution to the spectrum. However, small differences in binding energy, the limits imposed by linewidths, and by the resolution of our experiment would make their identification by curve fitting largely speculative. Thus, the analysis has been restricted to the contributions of aromatic carbon atoms (differentiating between C–C or C–H carbon atoms), methyl carbon atoms, and carbon atoms bound to nitrogen atoms. By applying constraints based on stoichiometry, electronegativity, and bond strength, the C 1s XPS spectra are best fitted by Voigt profiles (see Figure 1 for best-fit curves and Table S1 in the Supporting Information for best-fit parameters; a detailed description of the constraints implemented is given in the Supporting Information). Carbon atoms that belong to the aromatic rings and to the methyl groups contribute to the main line at lower binding energies, whereas those bound to nitrogen atoms show the second feature at higher binding energies, because of the electron-withdrawing effect of nitrogen atoms. It is also worth noting that three contributions to the main peak can be identified because of the signals from the C–C, the C–H, and CH_3 species (Figure 1, bottom). This assignment indicates a more efficient screening of the core hole in the internal ring C–C bonds, in agreement with previous work,[32–34] and may be attributed to cooperation in the screening of two adjacent rings, that is, improved charge delocalization along this channel.[34]

O 1s and N 1s core-level spectra can be used to ascertain if the paramagnetic function of this pyrene derivative is intact because the unpaired electron is delocalized over the two equivalent NO groups. Only one feature is observed in the N 1s and the O 1s core-level spectra, at 402.2 (Figure 1, top) and 531.3 eV (Figure 1, bottom), respectively. Both N 1s and O 1s spectra were fitted to a unique Voigt profile characterized by a constant Lorentzian width of 0.10 eV and a Gaussian width of 1.00 eV, in agreement with the intrinsic lifetime and inhomogeneous broadening found in the literature for core-hole states in organic molecules.[32,33] This indicates that the paramagnetic function of this pyrene derivative is intact and the degradation to iminonitroxide or to the diimmino derivatives[35] upon deposition (see Table S1 in the Supporting Information) can thus be excluded. The presence of an imino group as a degradation product would imply the presence of an XPS line at lower binding energy because breaking the nitrogen–oxygen bond hinders the electron-withdrawing action of the oxygen atoms, decreasing the binding energy[36] of the photoelectrons emitted from the N 1s core levels. This effect is observed in the XPS spectra of radiation-degraded molecules (see the Supporting Information).

XPS can also be used to obtain information on the nature of the interaction of the first layer of molecules with the substrate. The comparison of films of different thicknesses allows differentiation between chemi- and physisorption, and identifies the channel by which the core hole can be screened (pure molecular screening or substrate-improved efficiency of the screening effect).[33,37,38] In the present case, the C 1s, N 1s, and O 1s core-level spectra do not show significant differences as film thickness is increased. This observation excludes the occurrence of either chemical bonding to or strong interaction between **NitPyn** and the gold substrate (because both processes would deform the involved molecular orbitals leading to differences in the XPS features), and indicates that **NitPyn** molecules are weakly physisorbed on Au(111).

A pyrene molecule is 11.66 Å long, 9.279 Å wide, and 3.888 Å thick.[39] Thus, a 7 Å nominal thickness assembly of **NitPyn**, like that reported in Figure 1, is in the submonolayer regime, unless we assume that the molecules lie completely flat. XPS does not provide information on molecular orientation. However, recent preliminary X-ray absorption spectroscopy measurements indicate that the pyrene does not assemble lying flat on the substrate (see the Supporting Information).

The absence of relevant variations in the binding energies measured for the thinnest and the thickest layer (60 meV shift for C 1s) indicates that the screening of the core hole in the layer on the gold substrate is not efficiently assisted by the substrate. Efficient screening would be expected because at the metal–organic interface an additional screening of the core hole is present because of the occurrence of an image potential.[33,37] The observed behavior of the binding energy as a function of thickness suggests that the weakly physisorbed molecules are relatively distant from the substrate causing only a very small image potential.

We also observed that upon annealing at 550 K the molecules, including the monolayer, are completely desorbed from the Au(111) surfaces, confirming their very weak interaction with the gold substrate (see the Supporting Information). These observations are in agreement with the fact that pyrene has a very high vapor pressure at room temperature ($\approx 5.4\times10^{-4}$ Pa).[40] We assume that **NitPyn** also shows a similar value, slightly reduced by the presence of the radical moiety.[41] This implies that the molecules are extremely volatile at RT and have a relatively low tendency to adhere to and remain on a surface, as observed for molecules like perylene[11,12] and tetracene.[40] Under these conditions, a thermodynamic equilibrium between adsorption and desorption is established with no net growth on the surface. To obtain deposition from the vapor phase, it is necessary to work under nonequilibrium conditions. This is achieved by OMBD working under supersaturated conditions with the selected growth parameters.

The investigation of the growth modes of **NitPyn** on Au(111) under the present preparation conditions (0.7 Å min^{-1}

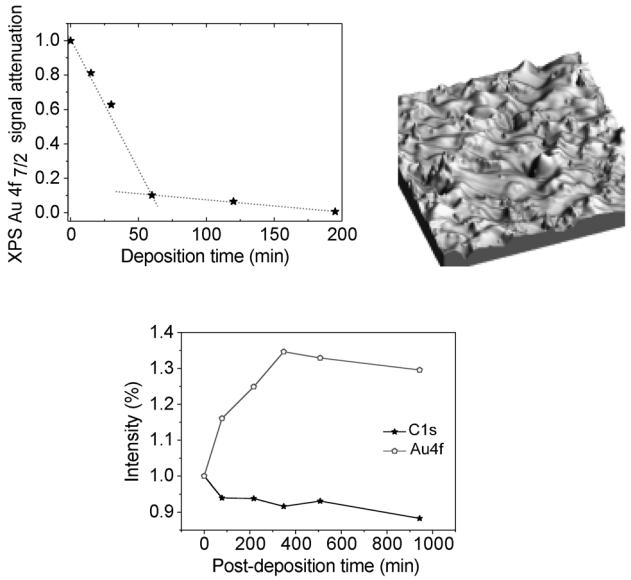

Figure 3. Attenuation of the Au 4f XPS signal, normalized to the corresponding saturation signal, as a function of time during **NitPyn** deposition on Au (111) at RT. The two gray dotted curves represent the best fit (top left). A typical 20 μm × 20 μm 3-dimensional AFM image of a **NitPyn** film after 120 min deposition (top right). Temporal evolution at room temperature of the Au 4f and C 1s XPS signals for a thicker film after deposition (bottom).

evaporation rate and substrate at RT) provides additional useful information. We monitored growth as a function of time by following the attenuation of the XPS substrate signal of the Au 4f peak (Figure 3, top left). The attenuation curve shows two different slopes with a crossover between the two regimes at 60 min (corresponding to a nominal thickness of 42 Å). This intensity trend hints at a Stranski–Krastanov growth mode (layer plus islands),[5] consistent with the AFM image (Figure 3, top right), clearly showing films with an island morphology.

Because of the high volatility of the molecules, we also monitored the system (49 Å nominal thickness) after deposition on gold by using XPS. Figure 3 (bottom) shows the time dependence of the Au 4f and C 1s signals. The relevant increase in the gold signal would suggest the desorption of the molecules from the substrate. However, this is not mirrored by the expected relative decrease of the C 1s signal, which shows only a 10% variation over 1000 min of monitoring (we also took care to minimizing beam exposure by switching the source off between measurements). Note that in UHV, the assembly seems to stabilize after 400 min.

This behavior can be explained by the occurrence of a slight desorption coupled with a substantial dewetting of the film at the interface. The dewetting possibly causes island ripening, that is, the adsorbed islands relax toward an equilibrium configuration to minimize their free energy. AFM investigations, although performed ex situ, indirectly support this statement, as we obtained different average roughness values (between 20 and 60 nm) measuring the same samples over several days (see the Supporting Information).

One of the major goals of the present work is to demonstrate that OMBD can be applied to organic radicals and in view of potential applications, we performed ESR measurements to investigate the persistence and the nature of the paramagnetic function of the molecule after deposition. The spectra of the residual powder left in the Knudsen cell after several cycles of heating/evaporation invariably showed a single exchange-narrowed line centered at $g = 2.00$. This provides evidence for the persistence of the paramagnetic character of the radical[42] (see the Supporting Information). However, these results do not exclude the presence of the imino nitroxide radical in the powder, a common degradation product of nitronyl nitroxide.[35] To clarify this point, we dissolved the residual powder in dichloromethane and recorded ESR spectra in liquid solution (Figure 4). These

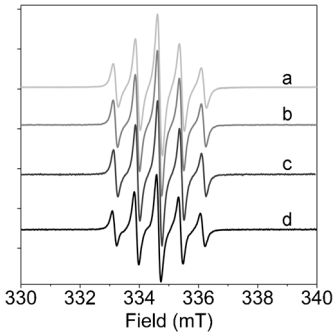

Figure 4. ESR spectra obtained from solutions in CH_2Cl_2 of the residual **NitPyn** powders present in the cell after a) two cycles, b) one cycle (residual power removed when the cell was at 325 K), c) one cycle (residual power removed when the cell was at RT), and d) the ESR spectrum of a solution obtained by washing one of the thin films.

showed the typical five-line pattern centered at $g = 2.009$ and a line–line separation of approximately 0.74 mT, indicating that the unpaired electron is delocalized over two equivalent nitrogen nuclei having $I = 1$. Together with the absence of the nine-line pattern expected for the imino nitroxide radical (see the Supporting Information), this result strongly indicates that the species after heating is an intact nitronyl nitroxide radical.

To study the magnetic features of the material after deposition we also investigated the solution obtained by washing the films from the substrate. These provided spectra with the same features discussed above (Figure 4), indicating that deposition occurs without degradation of the paramagnetic function of the molecules.

Consequently, a direct correlation between XPS and ESR results has been established. XPS spectra of stoichiometric films with intact molecules have always shown the expected ESR results, whereas the presence of additional features or different broadening in the core-level spectra, for example, as a consequence of radiation damage, were always mirrored in an ESR spectrum of the solution of the film washed from the substrate. These solution spectra show patterns different from the five-line pattern expected for an intact nitronyl ni-

troxide (see the Supporting Information). This correlation allows a very useful and powerful first screening by XPS in order to understand whether the magnetic properties of organic-based magnets are preserved in thin films.

Conclusion

We have successfully performed the deposition of **NitPyn** under strictly controlled conditions without degradation of the molecule. We have investigated the electronic properties, the chemical environment at the interface, and the growth mode of the obtained thin films. We have also demonstrated that evaporation and deposition on Au(111) single crystals under these preparation conditions do not affect the paramagnetic character of the molecules, suggesting the possible use of OMBD to grow films of organic-based magnets under controlled conditions and thus to use them as building blocks for new molecular devices.

The interface between **Nitpyn** and gold investigated in a clean environment is described and also discussed in terms of core-hole screening at the interface, distance of the molecules from the surface, mobility, desorption, and dewetting phenomena in purely organic-based magnets. These concepts are indispensable to the design and production of nanostructures for electronics.[9,10,43,44]

On the basis of the present results, and considering our previous knowledge of thin-film processes of organic molecules and factors that influence their growth, we are now able to predict the growth of **Nitpyn** on gold when varying the preparation conditions. Homogenous smooth films of parallel molecules are expected when the substrate temperature is kept lower than RT and increased grain size is expected when growing the assembly on substrates at temperatures higher than RT.[4,11,12,45] We note that lowering the substrate temperature may drastically reduce the azimuthal molecular order[11,12,41,45] and this may not represent an advantage when designing an active layer for electronics. On the other hand, higher substrate temperatures increase the desorption probability, rendering the necessary nonequilibrium conditions for deposition challenging. The use of larger polyaromatic substituents on radicals may solve these problems, intrinsically related to the thermodynamics and kinetics of **Nitpyn** film growth and evolution processes on gold substrates. Indeed, this would decrease their vapor pressure, favoring the growing of organized assemblies.

Experimental Section

Sample preparation and XPS measurements were performed in an UHV system consisting of a substrate preparation chamber and an OMBD-dedicated chamber, connected to an analysis chamber (base pressure 2×10^{-10} mbar) equipped with a SPECS Phoibos 150 hemispherical electron analyzer and a monochromatized X-ray source (SPECS Focus 500). A clean Au(111) single crystal (Mateck GmbH) was used as a substrate. The single crystal was prepared by Ar^+ ion bombardment (600 eV), followed by annealing in UHV at approximately 830 K. After several cycles of sputtering and annealing the substrate was checked for cleanness and structural properties with XPS and low-energy electron diffraction (LEED). Thin films of **NitPyn** were prepared in situ by OMBD (0.7 Å min^{-1} evaporation rate, substrate at RT). The evaporation rate was measured with a quartz crystal microbalance and the nominal thickness was cross-checked by using the attenuation of the XPS substrate signal (Au 4f) after **NitPyn** deposition. Survey XPS spectra were recorded with an electron pass energy of 50 eV; detailed spectra were measured with 20 eV for the C 1s core-level spectra and 50 eV for the O 1s and N 1s core-level spectra. The binding energy was calibrated by using the Au Fermi edge and the Au 4f XPS signals (Au $4f_{7/2}$ at 84 eV) as a reference.

NitPyn thin-films revealed radiation sensitivity on a relatively short time scale (several tens of minutes) shown by a clear broadening of the main lines and appearance of additional features upon strong X-ray exposure (see the Supporting Information). Thus, we have taken all precautions necessary to avoid radiation damaging (i.e., short beam exposure, short acquisition time, a freshly prepared film for each spectrum).

Atomic force microscopy studies were performed ex situ with a Digital Instruments Nanoscope III Multimode AFM. The experiments were carried out in tapping mode.

ESR spectra were performed at room temperature with an X-band Bruker Elexsys E500 spectrometer equipped with a high sensitivity ER4122 SHQE cavity (with a nominal weak pitch sensitivity of 3000:1).

For **NitPyn** synthesis, *N,N′*-dihydroxy-2,3-diamino-2,3-dimethylbutane (2.0 g, 13.5 mmol) was dissolved in methanol (50 mL) and 1-pyrenecarboxyaldehyde (3.3 g, 14.3 mmol) was added. The mixture was stirred rapidly at room temperature for several days and then poured into dichloromethane (300 mL) and cooled by use of an ice bath. Sodium periodate (11 g, 51 mmol) dissolved in water (110 mL) was then added, inducing a blue-violet coloration of the organic phase. The large excess of periodate is essential to obtain the radical and to avoid the formation of a yellow phase. The blue organic phase was separated and evaporated under vacuum, then purified by column chromatography with activated aluminum oxide/dichloromethane. A pure blue solution was obtained, which was gently evaporated under vacuum to give a greenish oil. This oil was subsequently redissolved in diethyl ether to obtain a blue solution. Blue-violet crystals were obtained by repeated recrystallization from diethyl ether. The molecular structure of this radical has been previously reported as a private communication to the Cambridge Crystallographic Database: C. Mann, R. Gompper, K. Polborn, 2003, CCDC-226038 contains the supplementary crystallographic data for this paper. These data can be obtained free of charge from The Cambridge Crystallographic Data Centre via www.ccdc.cam.ac.uk/data_request/cif.

Acknowledgements

The authors thank Wolfgang Neu for technical support, Dr. Heiko Peisert for providing the Knudsen cell, and Prof. D. Gatteschi for stimulating discussions. The Deutsche Forschungsgemeinschaft (DFG) under the contract CA852/5–1 is gratefully acknowledged. M.B.C. thanks the Wilhelm-Schuler-Stiftung for financial support. A.C., L.S., D.R., and M.M. acknowledge funding by Ente Cassa Risparmio di Firenze and the EU through the AdG ERC MolNanoM@s project (grant number 267746).

[1] F. Caruso, T. Hyeon, V. M. Rotello, *Chem. Soc. Rev.* **2012**, *41*, 2537.
[2] F. H. Jones, *Surf. Sci. Rep.* **2001**, *42*, 75.
[3] F. Morhard, J. Pipper, R. Dahint, M. Grunze, *Sens. Actuators B* **2000**, *70*, 232.
[4] a) J. A. Venables, *Introduction to Surface and Thin Film Processes*, Cambridge University Press, Cambridge, **2000**; b) J. A. Venables, *Surf. Sci.* **1994**, *299/300*, 798.
[5] E. Bauer, *Z. Kristallogr.* **1958**, *110*, 372.
[6] H. Brune, *Surf. Sci. Rep.* **1998**, *31*, 125.
[7] Z. Zhang, M. G. Lagally, *Science* **1997**, *276*, 377.
[8] C. Joachim, J. K. Gimzewski, A. Aviram, *Nature* **2000**, *408*, 541–548.

[9] F. Schreiber, *Phys. Status Solidi A* **2004**, *201*, 1037, and references therein.
[10] G. Witte, C. Wöll, *J. Mater. Res.* **2004**, *19*, 1889, and references therein.
[11] M. B. Casu, A. Schöll, K. R. Bauchspieß, D. Hübner, Th. Schmidt, C. Heske, E. Umbach, *J. Phys. Chem. C* **2009**, *113*, 10990.
[12] M. B. Casu, X. Yu, S. Schmitt, C. Heske, E. Umbach, *J. Chem. Phys.* **2008**, *129*, 244708.
[13] B.-E. Schuster, M. B. Casu, I. Biswas, A. Hinderhofer, A. Gerlach, F. Schreiber, T. Chassé, *Phys. Chem. Chem. Phys.* **2009**, *11*, 9000.
[14] a) H. Marchetto, U. Groh, Th. Schmidt, R. Fink, H.-J. Freund, E. Umbach, *Chem. Phys.* **2006**, *325*, 178; b) M. B. Casu, B.-E. Schuster, I. Biswas, C. Raisch, H. Marchetto, Th. Schmidt, T. Chassé, *Adv. Mater.* **2010**, *22*, 3740.
[15] D. Gatteschi, A. Cornia, M. Mannini, R. Sessoli, *Inorg. Chem.* **2009**, *48*, 3408.
[16] a) M. Mannini, F. Pineider, C. Danieli, F. Totti, L. Sorace, Ph. Sainctavit, M.-A. Arrio, E. Otero, L. Joly, J. C. Cezar, A. Cornia, R. Sessoli, *Nature* **2010**, *468*, 417; b) M. Mannini, F. Pineider, Ph. Sainctavit, C. Danieli, E. Otero, C. Sciancalepore, A. M. Talarico, M.-A. Arrio, A. Cornia, G. Gatteschi, R. Sessoli, *Nat. Mater.* **2009**, *8*, 194; c) A. Ghirri, V. Corradini, V. Bellini, R. Biagi, U. del Pennino, V. De Renzi, J. C. Cezar, C. A. Muryn, G. A. Timco, R. E. P. Winpenny, M. Affronte, *ACS Nano* **2011**, *5*, 7090.
[17] a) H. Wende, M. Bernien, J. Luo, C. Sorg, N. Ponpandian, J. Kurde, J. Miguel, M. Piantek, X. Xu, Ph. Eckhold, W. Kuch, K. Baberschke, P. M. Panchmatia, B. Sanyal, P. M. Oppeneer, O. Eriksson, *Nat. Mater.* **2007**, *6*, 516; b) S. Heutz, C. Mitra, W. Wu, A. J. Fisher, A. Kerridge, A. M. Stoneham, T. H. Harker, J. Gardener, H.-H. Tseng, T. S. Jones, C. Renner, G. Aeppli, *Adv. Mater.* **2007**, *19*, 3618.
[18] N. Domingo, E. Bellido, D. Ruiz-Molina, *Chem. Soc. Rev.* **2012**, *41*, 258–302.
[19] A. Cornia, M. Mannini, Ph. Sainctavit, R. Sessoli, *Chem. Soc. Rev.* **2011**, *40*, 3076.
[20] C. Simão, M. Mas-Torrent, N. Crivillers, V. Lloveras, J. M. Artés, P. Gorostiza, J. Veciana, C. Rovira, *Nature Chem.* **2011**, *3*, 359.
[21] M. Tamura, Y. Nakazawa, D. Shiomi, K. Nozawa, Y. Hosokoshi, M. Ishikawa, M. Takahashi, M. Kinoshita, *Chem. Phys. Lett.* **1991**, *186*, 401.
[22] J. H. Osiecki, E. F. Ullman, *J. Am. Chem. Soc.* **1968**, *90*, 1078.
[23] R. Chiarelli, M. A. Novak, A. Rassat, J. L. Tholence, *Nature* **1993**, *363*, 147.
[24] A. Caneschi, D. Gatteschi, R. Sessoli, P. Rey, *Acc. Chem. Res.* **1989**, *22*, 392.
[25] J. Veciana, H. Iwamura, *MRS. Bull.* **2000**, *25*, 41.
[26] M. Mannini, L. Sorace, L. Gorini, F. M. Piras, A. Caneschi, A. Magnani, S. Menichetti, D. Gatteschi, *Langmuir* **2007**, *23*, 2389.
[27] I. Ratera, J. Veciana, *Chem. Soc. Rev.* **2012**, *41*, 303.
[28] J. Lee, E. Lee, S. Kim, G. S. Bang, D. A. Shultz, R. D. Schmidt, M. D. E. Forbes, H. Lee, *Angew. Chem.* **2011**, *123*, 4506; *Angew. Chem. Int. Ed.* **2011**, *50*, 4414.
[29] J. Caro, J. Fraxedas, O. Jürgens, J. Santiso, C. Rovira, J. Veciana, A. Figueras, *Adv. Mater.* **1998**, *10*, 608.
[30] J. Caro, J. Fraxedas, A. Figueras, *J. Cryst. Growth* **2000**, *209*, 146.
[31] S. Molas, C. Coulon, J. Fraxedas, *CrystEngComm* **2003**, *5*, 310.
[32] A. Schöll, Y. Zou, M. Jung, Th. Schmidt, R. Fink, E. Umbach, *J. Chem. Phys.* **2004**, *121*, 10260.
[33] A. Schöll, Y. Zou, Th. Schmidt, R. Fink, E. Umbach, *J. Phys. Chem. B* **2004**, *108*, 14741.
[34] S.-A. Savu, M. B. Casu, S. Schundelmeier, S. Abb, C. Tönshoff, H. F. Bettinger, T. Chassé, *RSC Adv.* **2012**, *2*, 5112.
[35] E. F. Ullman, L. Call, J. H. Osiecki, *J. Org. Chem.* **1970**, *35*, 3623.
[36] G. Beamson, D. Briggs, *High resolution XPS of organic polymers: The Scienta ESCA300 database*, Wiley, New York, **1992**.
[37] M. B. Casu, *Cryst. Growth Des.* **2011**, *11*, 3629.
[38] D. Kolacyak, H. Peisert, T. Chassé, *Appl. Phys. A* **2009**, *95*, 173.
[39] L. C. Sander, S. A. Wise, *Special Publication 922*, *Polycyclic Aromatic Hydrocarbon Structure Index*, Chemical Science and Technology Laboratory, National Institute of Standards and Technology, Gaithersburg, **2011**.
[40] J. L. Goldfarb, E. M. Suuberg, *Environ. Toxicol. Chem.* **2008**, *27*, 1244.
[41] M. Müller, A. Langner, O. Krylova, E. Le Moal, M. Sokolowski, *Appl. Phys. B* **2011**, *105*, 67.
[42] J. A. Weil, J. R. Bolton, J. E. Wertz, *Electron Paramagnetic Resonance, Elementary Theory and Practical Applications*, Wiley, New York, **1994**.
[43] G. Heimel, I. Salzmann, S. Duhm, N. Koch, *Chem. Mater.* **2011**, *23*, 359.
[44] a) S. Braun, W. R. Salaneck, M. Fahlman, *Adv. Mater.* **2009**, *21*, 1450; b) J. Fock, M. Leijnse, K. Jennum, A. S. Zyazin, J. Paaske, P. Hedegård, M. Brøndsted Nielsen, H. S. J. van der Zant, *Phys. Rev. B.* **2012**, *86*, 235403; c) S. Müllegger, M. Rashidi, M. Fattinger, R. Koch, *J. Phys. Chem. C* **2012**, *116*, 22587.
[45] M. B. Casu, X. Yu, S. Schmitt, C. Heske, E. Umbach, *Chem. Phys. Lett.* **2009**, *479*, 76.
[46] A. Scholl, L. Kilian, Y. Zou, J. Ziroff, S. Hame, F. Reinert, E. Umbach, R. H. Fink, *Science* **2010**, *329*, 303.

Received: September 11, 2012
Published online: January 25, 2013

